Identification of a New Hormone-Binding Site on the Surface of Thyroid Hormone Receptor

P.C.T. Souza,* A.C. Puhl,* L. Martínez, R. Aparício, A.S. Nascimento, A.C.M. Figueira, P. Nguyen, P. Webb, M.S Skaf, and I. Polikarpov

Institute of Chemistry (P.C.T.S., L.M., R.A., M.S.S.), State University of Campinas-UNICAMP, Campinas, Sao Paulo, Brazil; Institute of Physics of São Carlos (A.C.P., A.S.N., P.W., I.P.), University of São Paulo-USP, São Carlos, Sao Paulo, Brazil; National Laboratory of Biosciences (A.C.M.F.), CNPEM, Campinas, Sao Paulo, Brazil; University of California Medical Center (P.N.), Diabetes Center, San Francisco, California; and Genomic Medicine (P.W.), Houston Methodist Research Institute, Houston, Texas

Thyroid hormone receptors (TRs) are members of the nuclear receptor superfamily of ligand-activated transcription factors involved in cell differentiation, growth, and homeostasis. Although X-ray structures of many nuclear receptor ligand-binding domains (LBDs) reveal that the ligand binds within the hydrophobic core of the ligand-binding pocket, a few studies suggest the possibility of ligands binding to other sites. Here, we report a new x-ray crystallographic structure of TR-LBD that shows a second binding site for T_3 and T_4 located between H9, H10, and H11 of the TRα LBD surface. Statistical multiple sequence analysis, site-directed mutagenesis, and cell transactivation assays indicate that residues of the second binding site could be important for the TR function. We also conducted molecular dynamics simulations to investigate ligand mobility and ligand-protein interaction for T_3 and T_4 bound to this new TR surface-binding site. Extensive molecular dynamics simulations designed to compute ligand-protein dissociation constant indicate that the binding affinities to this surface site are of the order of the plasma and intracellular concentrations of the thyroid hormones, suggesting that ligands may bind to this new binding site under physiological conditions. Therefore, the second binding site could be useful as a new target site for drug design and could modulate selectively TR functions. **(*Molecular Endocrinology* 28: 534–545, 2014)**

Thyroid hormone receptors (TRs) are members of the nuclear receptor (NR) superfamily of ligand-activated transcription factors that include the steroid, vitamin D, and retinoic acid receptors as well as "orphan" receptors for which there are no known ligand or function (1). Members of this class of proteins display a conserved structural organization consisting of an N-terminal transactivation domain (activation function [AF]-1), a highly conserved DNA-binding domain, and ligand-binding domain (LBD) in the carboxyl terminus. The LBDs are required for nuclear localization and homo- and/or heterodimerization and also contain a ligand-activated transactivation function (AF-2) that mediates the exchange of corepressor for coactivator (2). TRs are involved in cell differentiation, growth, and homeostasis (1). There are 2 TR subtypes, TRα and TRβ, which contain highly homologous DNA-binding domain and LBD sequences (3). The ligand-binding pockets (LBPs) of both subtypes differ only by a single amino acid residue (Ser277-TRα and Asn331-TRβ) (4). Although the main active natural TR ligand is T_3, the parental form of the hormone, T_4, can also bind TRs with lower affinity than

ISSN Print 0888-8809 ISSN Online 1944-9917
Printed in U.S.A.

Received November 6, 2013. Accepted February 3, 2014.
First Published Online February 19, 2014

* P.C.T.S. and A.C.P. made equal contributions to this work.

Abbreviations: ΔG, free energy difference; $\Delta\Delta G_{stat}$, statistical coupling parameter; ABF, adaptive biasing force; AF-1, N-terminal transactivation domain; AF-2, ligand-activated transactivation function; AR, androgen receptor; ER, estrogen receptor; H, α-helix; HT, 4-hydroxytamoxifen; LBD, ligand-binding domain; LBP, ligand-binding pocket; MD, molecular dynamics; NR, nuclear receptor; $N_{samples}$, minimum number of steps sampled; PDB, Protein Data Bank; PMF, $\Delta G(r)$ or potential of mean force; PPAR, peroxisome proliferator-activated receptors; S, β-strand; SCA, statistical coupling analysis; TR, thyroid hormone receptor; VDR, vitamin D receptor.

T_3 and, because the total serum T_4 is 40-fold higher than T_3 (1), there have been suggestions that T_4 could modulate TR activity (5). TRβ is found predominantly in the liver, being involved with regulation of metabolic rate and hepatic cholesterol metabolism, whereas TRα is found particularly in the heart and plays a major role in regulation of heart rate (6, 7). Selective TRβ1 modulators increase metabolism, improve lipid balance, and prevent deleterious effects on the heart. This class of compounds has been considered very useful in the treatment of obesity and hypercholesterolemia, and many efforts have been devoted to find a good selective modulator molecule (8–11).

Like other NR family members, TR LBDs are folded into 3 layers of α-helices that form the hydrophobic core of the molecule, where the ligand is buried. The TR LBD changes conformation upon agonist binding. This conformational alteration results in a folding pattern consistent with various members of the nuclear receptor superfamily, suggesting a similarity between NR LBD ligand-binding mechanisms (12). The ligand induces tight packing of the LBD C-terminal helix 12 (H12) against the body of the receptor (12, 13). Molecular dynamics (MD) simulations and new experimental results have expanded this view, showing that there may be multiple pathways of ligand entry and exit (14–21).

H12 contributes to ligand binding when it is stabilized in active conformation, by forming additional ligand-protein and intraprotein interactions (22). The repositioning of H12 causes major rearrangements of H11, loop H11–H12, and the connection between H1 and H3 occur. This rearrangement of H12 induces formation of coactivator-binding site motif LXXLL on the liganded NR surface (residues in helices H3, H4, H5, and H12 itself) that generates the transcriptional activity of the AF-2 domain of nuclear receptors, thereby influencing gene expression (23). Thus, this ligand-regulated protein-protein interaction is critical to mediate transcriptional activation, and helix H12 is a crucial component of the NR LBD because it controls agonist/antagonist properties of NRs (24, 25). A recent study demonstrated that apo-TR H12 in inactive (and antagonist) conformation is docked in the C-terminal part of H3, blocking coactivator and corepressor interface and suggesting a new mechanism of self-inactivation for TR (26).

Although X-ray structures of many NR-LBDs reveal that the ligand binds within the hydrophobic core of the domain, some other binding sites have been observed for small molecules. For example, it was shown that the estrogen antagonist 4-hydroxytamoxifen (HT), in addition to occupying the core binding pocket within the LBD of estrogen receptor (ER) β, could also bind to a second site on its surface. This crystal structure revealed one HT molecule bound to the consensus LBP and another bound to a site that overlaps with the hydrophobic groove of the coactivator recognition surface (27). The second binding site for HT was previously reported in studies of sedimentation patterns. It was demonstrated that, despite the receptor's high affinity for HT, the total binding for HT was nearly twice the one of estradiol (28). It was proposed that that the primary, high-affinity site was responsible for agonist activity of the antiestrogen, whereas the secondary, low-affinity site was responsible for antagonist activity (29). A noncanonical binding pocket was also observed for androgen receptor (AR) and termed BF3 (30–32). At least 3 different ligands were identified with the ability to bind to this site and weaken coactivator interaction, thus functioning as AR inhibitors with decreased capacity of antiandrogen resistance development (32). Curiously, BF3 is located in a different region of AR LBD, next to the AF-2 region, but without overlap with the coregulators groove (30).

Another example is the alternative ligand-binding site of the vitamin D receptor (VDR), identified by computational modeling. Data obtained from docking experiments generated a receptor conformational ensemble model that could explain how VDR and possibly ER can have genomic and nongenomic functions. The new alternative site partially overlaps with the canonical LBP, not allowing 2 ligands simultaneously associated with VDR (33). For peroxisome proliferator-activated receptors (PPARs), the presence of more than one ligand bound to the LBD has already been shown by X-ray crystallography studies (34–37). The additional ligands bind cooperatively in the large LBP of PPARs. An exception is PPARγ associated with ajulemic acid. The crystallographic structure of this complex shows 2 molecules of this ligand bound to LBD, one being anchored to the coregulators interaction groove (38), such as the second HT molecule bound to ERβ (27). The same region has been successfully used for the design of irreversible TR antagonists (39–41).

In the present study, we used X-ray crystallography to identify a new second binding site for T_3 and T_4 within the LBD of TRα. T_3 and T_4 associate with a secondary site located between H9, H10, and H11. The main interactions between the second T_3/T_4 and the LBD are polar contacts. H12 did not alter its position because of the presence of a second hormone molecule. Statistical multiple sequence analysis indicates coupling between amino acid residues of the first, internal hormone-binding site and the second, surface-binding site. We also conducted extensive MD simulations that enabled us to investigate the mobility, interaction energies, and the binding modes

of the ligands in the surface binding site and to compute an estimate of the binding free energy. Furthermore, we probed amino acid residues of the new ligand-binding site using site-directed mutagenesis and functional assays. Collectively, these results indicate that the second binding site of TR should exist under physiological conditions and might be relevant for its function.

Materials and Methods

Expression and purification

The plasmid PET28a(+) (Novagen) encoding a human TRα1 LBD construct fused in frame to the C terminus of a polyhistidine (His) tag was expressed in *Escherichia coli* strain B834. The protein was expressed and purified according to previous studies (42). Proteins were resuspended in a solution of 600 mM NaCl and 3 mM dithiothreitol and further concentrated to 10 mg ml^{-1}. The protein content and purity of all chromatographic fractions were analyzed by Coomassie Blue-stained SDS-PAGE. Protein concentrations were determined using the Bradford dye assay (Bio-Rad Laboratories) using BSA as standard, and the average yield of the protein was about 6 mg per liter of culture.

Crystallization, data collection, and structure determination

Crystallization screens were performed according to previous studies (42). In each trial, a hanging drop of 1 μL of hTRα LBD solution containing 10× molar excess of either T_3 or T_4 was mixed with 1 μL precipitant solution and equilibrated against a reservoir containing 500 mL precipitant solution. Suitable crystals were grown within 1 day with 0.1 M sodium cacodylate (pH 6.5), 1.4 M sodium acetate. Further optimization led to X-ray diffraction quality crystals of hTRα grown in 1.0 M sodium cacodylate and 0.1 M sodium acetate threehydrate (pH 7.2) within 24 hours at 291 K. The crystals grew in orthorhombic $P2_12_12_1$ space group. Before data collection, crystals were soaked in cryoprotectant solutions containing 1.0 M NaCac, 0.1 M NaH_3OAc (pH 7.2) and 20% (vol/vol) ethylene glycol and rapidly cooled in a gaseous nitrogen stream at 100 K. X-ray diffraction experiments were performed with a MAR research MAR345dtb image-plate detector mounted on a Rigaku UltraX 18 rotating-anode X-ray generator providing Cu Kα radiation operated at 50 kV and 100 mA and equipped with Osmic confocal Max-Flux optics. The data sets were reduced, merged, integrated, and scaled using DENZO and SCALEPACK softwares (43).

The structures were determined by molecular replacement using AMORE. The TRβ LBD+T_3 (PDB code: 1BSX) structure was used as a model for molecular replacement (44). For the refinement cycles and model building, we employed PHENIX (45), REFMAC5 (46), and COOT (47).

Statistical coupling analysis (SCA)

SCA was performed with a multiple sequence alignment of NR-LBDs from several species to analyze site conservation (ΔG^{stat}) and statistical coupling ($\Delta\Delta G^{stat}$) parameters of the second binding site. The multiple sequence alignment was downloaded from the Pfam server (http://www.sanger.ac.uk/Software/Pfam/) and edited with the Jalview program (48) to remove gaps and redundancy at a cut-off of 95%, remaining in the final alignment 1297 protein sequences. The SCA was conducted as previously described (49, 50). The matrix containing all performed perturbations was subjected to successive rounds of clustering rows and columns with similar $\Delta\Delta G^{stat}$ distribution using the software package MATLAB (The Mathworks, Inc) and after each cycle, positions with weak signals were discarded. All the results shown in this work are reported on human TRα (PDB code 2H79).

Site-directed mutagenesis and cell transactivation assays

The residues of the second binding site were submitted to site-directed mutagenesis using QuikChange site-directed mutagenesis kit according to the manufacturer's instructions (Stratagene). Single-point mutations were introduced (D382R, E393R, Q396R, and R429A) at the LBD of the nuclear receptor TRß1 cloned into pCMV mammalian expression vector plasmid. The presence of the mutations was verified by DNA sequencing. The conservation of the TRα and TRβ LBDs is high, and these mutated residues are conserved (3).

For transactivation assays, U2-OS cells were seeded into 24-well plates at density of 1×10^5cells/well and grown in 10% FBS-DMEM supplemented with 2 mM glutamine and 50 μg/mL streptomycin under 95% air and 5% CO_2 at 37°C overnight. The cells were then cotransfected with 10 ng of pCMV-TRβ1 or mutants and with 100 ng thyroid response element (DR4 or F2)-linked luciferase reporters. The plasmid pRL containing the *Renilla* luciferase gene was transfected simultaneously acting as the transfection control. TransFectinβ Lipid Reagent (Bio-Rad Laboratories) was mixed with plasmids in DMEM and incubated at room temperature for 20 minutes prior to adding to the culture media. The ratio of DNA (micrograms) to TransFectin (microliters) was 1:3. T_3 or T_4 was added to the culture media 4 hours later and incubated with the cells overnight. The cell monolayer was then washed with PBS and harvested with lysis buffer (Dual-Luciferase Report Assay system; Promega Corp.), following the manufacturer's instructions. Luciferase activity of the cell lysate was determined using the Luciferase Assay System (Promega) and measured in a Safire (2) luminescent counter (Tecan; Tecan US). The *Renilla* luciferase activity was measured using the same cell lysate (Dual-Luciferase Report Assay system; Promega) functioning as an internal control for the corresponding luciferase activity to adjust variation caused by transfection efficiencies (51).

Molecular dynamic simulations

The initial configurations for TRα LBD complex were obtained from crystallographic structures reported here (with T_3 and T_4 in the second binding site) and from Protein Data Bank (PDB code 3GWS; without ligand in the second binding site). The complete simulated systems were built with Packmol (52, 53) containing the TRα LBD complex, water, and one counterion for each charged residue for electroneutrality (42 Na^+ and 30 Cl^- ions). We used a cubic box with 16 600 water molecules with side dimension of 81 Å, leading to a 15 Å hydration layer in average. A time-step of 2.0 fsec and the velocity Verlet algo-

rithm (54) were used. A 14-Å cutoff with smooth switching function starting at 12 Å was applied for the Lennard-Jones interactions, whereas electrostatic forces were treated via the particle mesh Ewald sum method (55). Minimization and equilibration were performed as follows. The energy of the system was minimized by 700 conjugate gradient (CG) steps, keeping all protein atoms fixed. Fixing only the Cα atoms, another 500 CG steps were performed. Finally 300 CG steps were carried out without any restrictions. After minimization, 2 nsec equilibration MD simulations were performed under constant temperature and pressure conditions (298 K and 1 bar), with Langevin thermostat and barostat. The damping coefficient of Langevin thermostat was 5 $psec^{-1}$. The oscillation period and decay time of the piston in Langevin barostat was 200 fsec and 100 fsec, respectively. The production MD simulations at constant temperature and pressure were performed after this protocol, lasting 6 nsec.

These procedures were repeated 6 times for each of the following systems: 1) TRα LBD with T_3 in first and second binding sites (TRα-T_3-T_3); 2) TRα LBD bound to T_3 and T_4, respectively in the first and in the second binding site (TRα-T_3-T_4); 3) TRα LBD without any ligand in second binding site (TRα-T_3). Auxiliary MD simulations were performed with another system: TRα-T_3 with tyrosine amino acid bound to the second binding site (TRα-T_3-TYR). Tyrosine is a precursor to thyroid hormones, thus having a similar molecular structure. Furthermore, this amino acid has plasma and intracellular concentration higher than the thyroid hormones. These features suggest TYR as a possible natural ligand of the second binding site. The same procedures described above were used to test this hypothesis, but with 2 nsec production MD simulations.

All simulations were performed with NAMD 2.7 (56), applying the CHARMM 27 force field for proteins (57) and the TIP3P model for water (58). The ligands (T_3 and T_4) were parameterized in order to describe the molecular geometry, theoretical and experimental torsional barriers (59, 60), and the partial atomic charges in water solution, following a similar protocol used for other biomolecules (21, 61, 62).

Free energy calculations

To investigate the binding free energy of T_3 and T_4 to the second binding site, the order parameter (or "reaction coordinate") was chosen as the distance (r) separating the center of mass of the ligand from a dummy atom placed within the bulk solution. Rotations and translations of the LBD were avoided by applying soft harmonic potentials to all α-carbons 20 Å from the second binding site residues.

The dependence of the free energy with ligand displacement (the $\Delta G(r)$ or potential of mean force [PMF]), from 0 to 15 Å relative to the reference-bound position, was determined using the Adaptive Biasing Force (ABF) method, implemented in NAMD (63, 64). The initial structure of the protein was obtained from the last step of one of the equilibrium MD simulations described above. A cubic box with 18 600 water molecules with side dimensions of $97 \times 76 \times 80$ Å was used. Instantaneous values of the force were accrued in bins 0.1 Å wide. Boundary potentials with a force constant of 10 kcal/mol/$Å^2$ were also used. These parameters appear to constitute reasonable choices in other free energy calculations using the ABF method (63–65). For each system (TRα-T_3-T_3 and TRα-T_3-T_4), 2 simulations were done initially: 1) 25 nsec ABF simulation with a minimum number of steps sampled ($N_{samples}$) collected before the full application of ABF force; and 2) 40 nsec ABF simulation with $N_{samples} = 10\,000$.

No substantial change was observed in the final values of ΔG obtained with different $N_{samples}$ used. However, differences were noted in some regions of PMF curves. To enhance sampling in these regions, three additional 20 ns ABF simulations with $N_{samples} = 2000$ were made for each system in 3 intervals: $0 \leq r \leq 3$ Å; $2.5 \leq r \leq 6.5$ Å; and $6 \leq r \leq 11$ Å. The PMF curve of each system was calculated as the average of the 5 simulations. The average was done by weighting the samples of the dG/dr from each bin of the simulations.

Results

Thyroid hormones can bind to a second binding site on the surface of TR

The structures of the TRα LBD in complex with T_3 and T_4 exhibited the classical 3-layered α-helical sandwich conformation, composed of 12 α-helices, H1–H12 and 4 short β-strands, S1–S4 similar to other TRα and -β structures (4, 5, 66, 67). Cocrystallization of TRα with T_3 and T_4 yielded structures with good geometric and crystallographic parameters. The Ramachandran plots were acceptable for both structures, and no residues were observed in the disallowed region of the plots. The crystals contained one single TR molecule in the asymmetric unit organized in the orthorhombic form (Table 1). In each structure, 2 molecules of hormones per TRα were observed in the electron density. For both complex structures, 1 molecule of hormone is located in the LBP and the other one is found in a second binding site, clearly indicated by the electron density map, located between helix H9, H10, and H11 (Figure 1 and Figure 2). In the case of the LBD structure of TRα-T_3-T_3, the coordinates of the iodine atoms in both binding sites were confirmed with the use of anomalous maps composed with the refinement phases and anomalous signal from the iodine atoms. In the structure TRα-T_3-T_4, anomalous maps confirmed the presence of 4 iodines in the second binding site and 3 iodines in the canonical binding site. Interestingly, in the latter, indication of the presence of a fourth iodine atom was obtained with a signal/noise approximately 10 times lower then the iodine with the highest occupancy. Attempts to refine this fourth iodine were unsuccessful.

In the LBP, the ligand is completely enclosed within the core of the LBD and exhibits a similar binding mode, as described in other TR-T_3 and TR-T_4 structures (5, 66). The thyroid hormones interact with the LBP by a hydrogen bond between a hydroxyl group and H381, a hydrogen bond between a carboxyl group and R228 and, also, by hydrophobic contacts of thyronine rings and apolar residues. The difference is that R228 seems to present an

Table 1. Crystallographic Information: TRα in Complex with T_3 and T_4

Data Collection	TRα-T_3,T_3 Complex	TRα-T_3,T_4 Complex
Space group	$P2_12_12_1$	$P2_12_12_1$
Unit cell parameters		
a (A°)	59.78	59.74
b (A°)	80.79	80.92
c (A°)	102.56	101.87
ASU content (molecules)	1	1
Resolution range (A°)[a]	63.246 − 1.90 (2.00 − 1.90)	63.246 − 2.05 (2.16 − 2.05)
Unique reflections	39 906	31 309
Wavelength (Å)	1.5418	1.5418
Multiplicity [a]	8.0 (8.0)	14.6 (14.9)
Completeness (%)[a]	99.9 (99.9)	98.9 (97.6)
R_{merge} (%)[a,b]	0.051 (0.349)	0.068 (0.375)
Mean I/σ(I) [a]	25.6 (4.9)	31.8 (6.9)
Bfactor from Wilson plot (Å^2)	28.62	30.00
Refinement Statistics		
R_{factor}[c]/R_{free}[d]	0.1582/0.1843	0.1553/0.1773
RMSD from ideality		
Bond lengths (Å)	0.009	0.010
Bond angles (°)	1.321	1.375
Ramachandran analysis		
In preferred regions (%)	96.55	97.11
In allowed regions (%)	3.45	2.89
Outliers (%)	0	0
PDB code	4LNW	4LNX

Abbreviation: ASU, asymmetric unit; RMSD, root mean square deviation.

[a] Values in parameters refer to the last resolution shell.

[b] R_{merge}: $\sum_{hkl,j}(I_{hkl} - \langle I_{hkl}\rangle)/\sum_{hkl,j} I_{hkl}$, where $\langle I_{hkl}\rangle$ is the average intensity for a set of j symmetry-related reflections, and I_{hkl} is the value of the intensity for a single reflection within a set of symmetry-related reflections.

[c] R_{factor}: $\sum_{hkl}(F_o - F_c)/\sum_{hkl} F_o$, where F_o is the observed structure factor amplitude, and F_c is the calculated structure factor amplitude.

[d] R_{free}: $\sum_{hkl}T(F_o - F_c)/\sum_{hkl} F_o$, where a test set, T (5% of data), is omitted from the refinement

alternative conformation in the structure when T_3 is present in the second binding site (discussed below).

In the second binding site, T_3 and T_4 interact with the protein mainly by polar interactions between residues Q342 (located in the helix H10, Q396 in TRβ1) and R375 (located in helix H11, R429 in TRβ1) and apolar interactions with S326, V371, T372, L346, and L368 (Figure 2). The carboxylic head of the ligand points toward residue R375, whereas Q342 establishes a salt bridge between its amide group and T_3 amino and carboxylic groups. Hydrophobic residues between helices H9 and H10 also create an appropriate surface for ligand positioning.

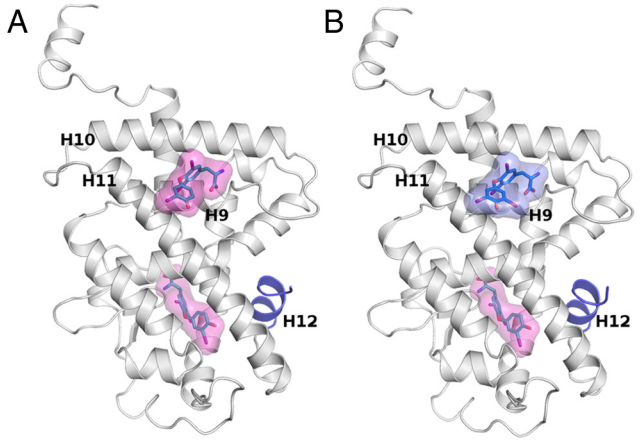

Figure 1. Crystal structure of TRα LBD complexes. A, The overall structure of TRα with two T_3 molecules bound. The T_3 bound to the second binding site is located in the upper part. B, The overall structure of TRα with T_3 and T_4 molecules bound. The T_4 bound to the second binding site is located in the upper part between helix H9, H10, and H11. H12 is in blue in both structures.

TRα and TRβ canonical LBPs differ by a single residue (Ser277 in TRα and Asn331 in TRβ). However, the main residues responsible for ligand interaction with the second binding site are conserved. Thus, a second T_3 or T_4 might also bind to TRβ. Borngraeber et al (68) previously observed electron density for a second GC-24 molecule in the potential dimerization interface of TRβ. This result was considered a crystallization artifact, and the electronic density was modeled in the pocket formed by helices H1, H2, H8, and H9. We refined the structure placing the GC-24 in the crystallographic symmetric position, which corresponds approximately to the second site proposed here. The final model has an R_{factor} and R_{free} that converged at 0.218 and 0.250, respectively. Supplemental Figure 1, published on The Endocrine Society's Journals

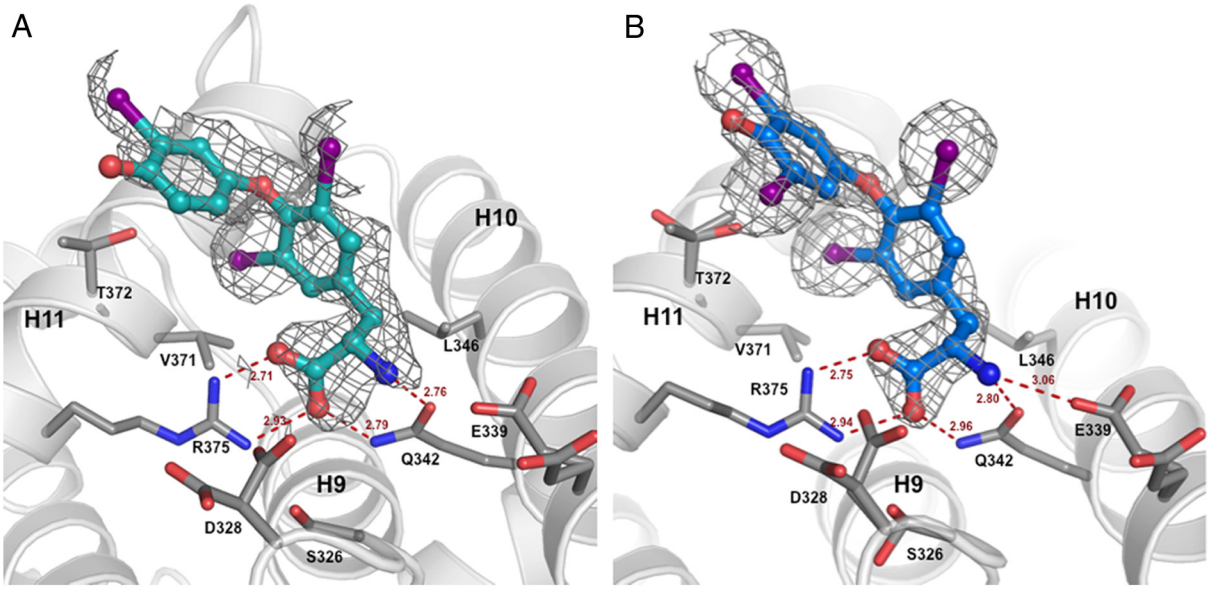

Figure 2. Electron density map of a second bound T_3 and T_4 in TRα receptor. A, Electron density map and polar interactions of T_3. B, Electron density map and polar interactions of T_4. A σ-weighted 2 *Fo-Fc* omit electron-density map is shown contoured at 1.0 σ for the area surrounding the T_3 and T_4 ligands. The T_3 and T_4 are colored by element. The amino acid residues that interact with the ligands are labeled and displayed as sticks.

Online web site at http://mend.endojournals.org, shows GC-24 bound to the second binding site in TR. The phenol group of the second GC-24 molecule interacts with Q396 in H10, which corresponds to residue Q342 in TRα, resembling the interaction of T_3 and T_4 in the second binding site observed in our structures.

Residues of the second binding site are coupled with relevant function regions and are important for transactivation of the TR

Statistical coupling analysis (SCA) was already shown to be an efficient technique to identify the positions that have been functionally constrained during evolution. Here we analyzed a multiple alignment of the NR's LBD looking for statistical couplings involving the residues interacting with the second binding site. If 2 positions have high $\Delta\Delta G^{stat}$, these positions suffered correlated mutations during evolution, which can reveal functional correlations within substructures of the protein (49, 50). An analysis of $\Delta\Delta G^{stat}$ computed from our sequence alignment revealed a number of coupled positions, shown in a matrix form in Figure 3. The TRα residues Q342, E339, and R375 that make polar contacts with T_3 and T_4 in the second binding site show coupling with each other and with several positions identified by SCA, such as R266 (LBP) and L374 (H11-dimerization interface). Moreover, residues Q342, E339, and R375 are also coupled to amino acids located at the hydrophobic groove, responsible for interactions with coregulators (A233 and K234, at H3; F239 at H5; Q247 and K252, at H5); position L400 (H12), and the charge clamp residues K234 and E403, involved in activation function 2 (AF-2). These results indicate that residues making up the second binding site could be important for allosteric mechanism.

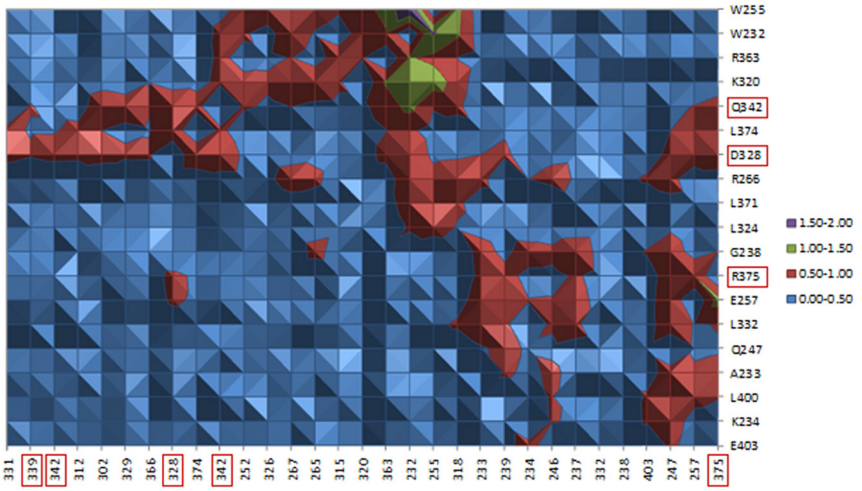

Figure 3. Matrix of $\Delta\Delta G^{stat}$ values reporting coevolution of many pairs of positions in an alignment of 1237 members of the NR_LBD family after cluster analysis. Rows in the matrix represent LBD positions and columns represent perturbations. The color scale ranges from white for small $\Delta\Delta G^{stat}$ values to dark red for high $\Delta\Delta G^{stat}$ values. The residues of the TR second binding site are highlighted in the graph axes.

Our analyses also indicated a regulatory role of the second site on the TR activity, as shown for F2- and DR4-dependent reporters in Figure

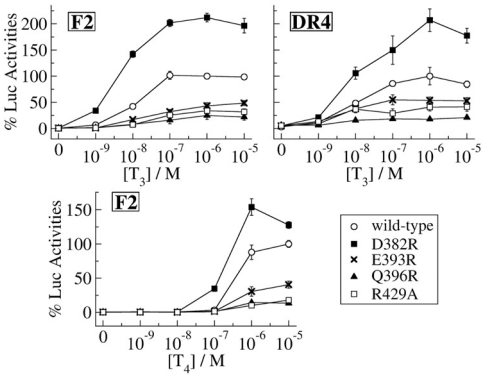

Figure 4. TRβ1/luciferase transactivation assays of T_3 and T_4 doses at F2 and DR4 response element-dependent reporters. The cells are transfected with wild-type TRβ1 and single-point mutations in residues of the second binding site (D382R, E393R, Q396R, and R429A). The activities are expressed relative to the maximum response of the wild-type (concentration of 10^{-6} M to T_3 and 10^{-5} M to T_4), which is set to 100%. Error bars represent the SDs of at least 4 experiments, being featured only values above 4%.

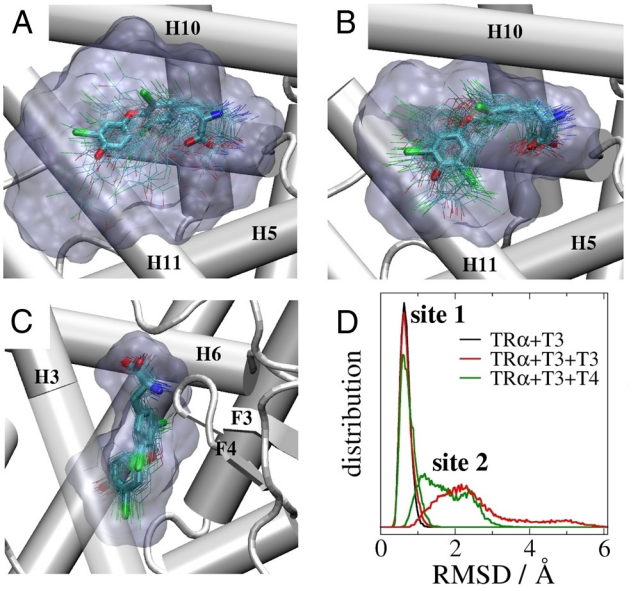

Figure 5. MD simulations show a high mobility of the ligands in second binding site. The first two pictures show the superposed configurations and the corresponding average occupied volume of T_3 (A) and T_4 (B) in the second binding site. The same analysis for T_3 in the first binding site is shown in panel C. T_4 is less mobile than T_3 in second binding site, and both are more mobile than T_3 in the first binding site. Distributions of root mean square deviation (RMSD) (D) of natural ligands in the first and in the second binding sites show quantitatively the results presented in the previous figures. Interestingly, T_3 is more mobile in the first binding site when there is a ligands bound to the second site.

4. For example, T_3 dose-response curves at the F2-dependent reporter show that the mutant R429A, in which the arginine that interacts to the carboxylate portion of ligands is substituted by an alanine, exhibits just 35% of wild-type TRβ1 maximum response. Likewise, E393R and Q396R mutations also exhibit reduced transcriptional activity (50% and 25%, respectively). In contrast, the mutant D382R, in which one of the aspartic acids that makes a salt bridge with T_3 is changed to arginine, exhibited an increase in transcriptional response (212% of the maximum wild-type TRβ1 activity). The results obtained for T_3 at DR4 and T_4 at F2 exhibit the same trends.

MD simulations show a mobile and high-affinity second binding site

MD simulations of 3 different systems were performed: TRα LBD bound with T_3 in the second binding site (TRα-T_3-T_3), TRα LBD bound with T_4 in the second binding site (TRα-T_3-T_4), and TRα LBD without ligand in the second binding site (TRα-T_3).

The results of these simulations show that T_4 is less mobile than T_3 in the second binding site (Figure 5, A, B, and D), but both have high mobility compared with T_3 in the LBP (Figure 5C). The phenolic ring is the most mobile part of T_3 or T_4 in the second binding site. Unlike in the LBP, the phenol group of the hormones does not make polar interactions with the LBD.

The LBD-ligand interaction energies reflect the high mobility of ligands on the second binding site, denouncing the existence of multiple binding modes (Figure 6, A and C), hereafter denoted as strong mode (I), dynamic mode (II), and weak mode (III). The main residues that interact with ligands on the second site are E339, Q342, and R375 (TRα, Figure 6B). In addition to these, smaller contributions come from the negatively charged residues D328, D336, and E343. Additionally, there is a large fluctuation of the D328-ligand interaction energy, which can even result in unfavorable (positive) interactions.

T_4, which is less mobile than T_3 in the second binding site, does not display the weak mode, and the interaction energies of the dynamic mode are more favorable than the T_3 ones (Figure 6A). We believe that this is because T_4 is more hydrophobic, thus improving its attachment to the LBD. On average, the LBD-ligand interaction energies of T_4 and T_3 in the second binding site are -150.70 and -120.6 kcal.mol^{-1}, respectively. These interaction energies indicate that T_4 has higher affinity than T_3 to the second binding site.

Because the measurement of TR-ligand affinity in the second binding site is essential to verify the possibility of this site actually existing in physiologic solution, we performed extensive MD simulations (~125 nsec for each system) using the ABF method to obtain an estimate of the binding free energy of each ligand. Figure 6D shows the free-energy profile corresponding to the dissociation of the ligand. The free-energy difference between ligand bound and unbound states obtained for T_3 and T_4 was $\Delta G = -9.6$ and -14.2 kcal.mol^{-1}, respectively. These

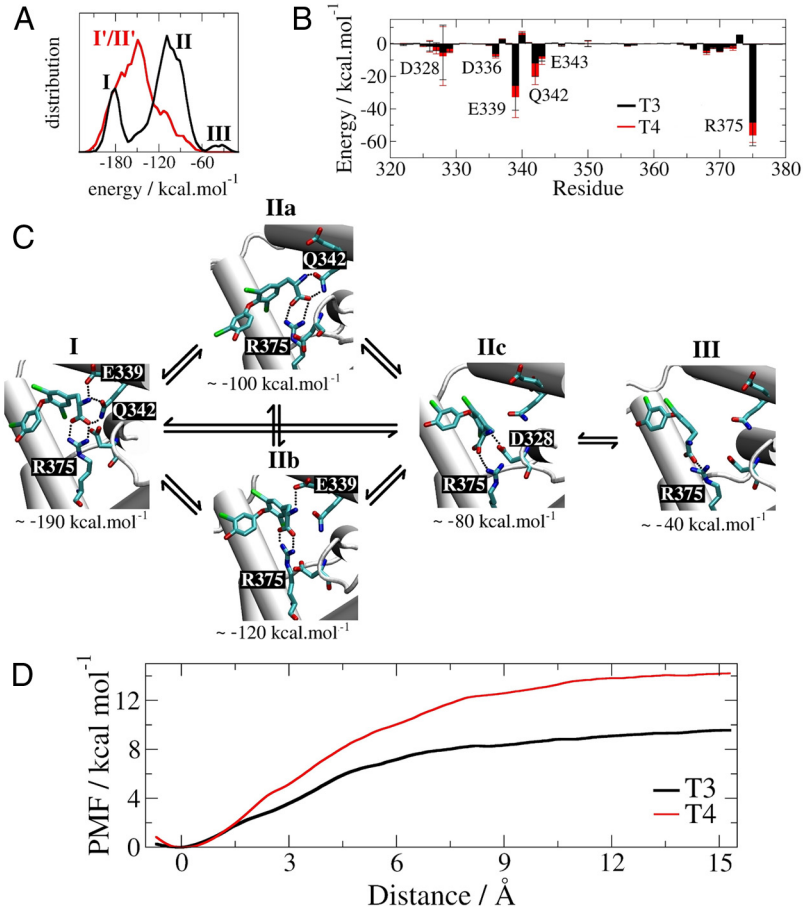

Figure 6. Multiple binding modes of the ligands in the new site and estimates of the $\Delta G_{binding}$. A, Distributions of the LBD-ligand interaction energy of T_3 (black) and T_4 (red) in the second binding site. B, Average interaction energy between the ligands and principal residues in the second binding mode. C, The multiple binding modes of T_3 and its complex interconversion. T_3 clearly shows 3 binding modes with different interaction energies: strong mode (I), dynamic mode (II), and weak mode (III). D, The free energy change (or PMF) for the ligand dissociation of the second binding site obtained by Adaptative Biasing Force (ABF) method. The final $\Delta G_{binding}$ of T_3 and T_4 was approximately −9.5 and −14.2 kcal.mol^{-1}, respectively.

correspond to binding affinities (K_d) of 90.9 nM for T_3 and 0.04 nM for T_4. These results are consistent with observations from equilibrium MD simulations, which already indicated that T_4 has greater affinity than T_3 for the second site.

Other biomolecules present in higher concentrations could also be potential second-site ligands. Auxiliary MD simulations were performed to evaluate the possibility of the amino acid tyrosine acting as a ligand for the second binding site, but tyrosine does not display a stable attachment to the site and dissociated from it in all simulations (Supplemental Figure 2).

Influence of the second site in the structure, dynamics, and interactions of the first site

Binding of T_3/T_4 to the second binding site may be associated with alterations of the structure and dynamic behavior of the LBD. Our equilibrium MD simulations did not show any significant differences in backbone mobility. However, we observed that the ligand in the LBP has a slightly higher mobility when the ligand is present in the second binding site, as shown by the root mean square deviation peaks in Figure 5D. The average interaction energies also show that the interactions of T_3 in the first binding site with the protein are less favorable when a ligand is bound to the second site: −124.2 kcal.mol^{-1} for TRα-T_3; −113.8 kcal.mol^{-1} for TRα-T_3-T_3; and −116.2 kcal.mol^{-1} for TRα-T_3-T_4.

These changes are related to the reduced interactions of T_3 with R228, one of the main residues in the LBP that may interact with the solvent, as indicated by MD simulations of systems containing ligands in the second binding site. Although infrequent, this change in the side-chain position is consistent with the 2 conformations of R228 observed in the crystallographic structure with T_3 in the second binding site (Figure 7). In the TR crystallographic structure with T_4 in the second site, this alternative electron density seems to be better fitted by a water molecule in this region. However, the possibility of a second R228 conformation cannot be ruled out in this case also. These results indicate that ligands on the second binding site may influence ligand-protein interactions in the LBP.

Discussion

In this study, we used X-ray crystallography to obtain new structures of the TRα LBD associated with the natural thyroid hormones, T_3 and T_4. Surprisingly, we observed 2 ligand molecules associated with the TRα LBD, one anchored to the conventional LBP and another in a new second binding site, located on the surface of the protein, between H9, H10, and H11. Except for the second hormone molecule, the structure appears very similar to other TR LBDs associated with agonist ligands, in which H12 is in appropriate position for interaction with

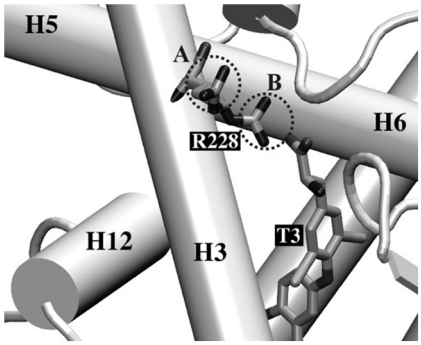

Figure 7. Two conformations of R228, one of the main residues in the cognate binding site, observed in the crystallographic structure with T_3 in the second binding site. A, R228 exposed to the solvent and (B) interacting with the ligand. MD simulations also reveal these 2 conformations.

coactivators (4, 5, 66, 67). Until now, this second binding site had never been reported for other NR structures. However, the structure refinement of TRβ1 LBD associated with two GC-24 molecules, one of them on the symmetrical position, shows the existence of a second binding site at another crystallographic NR structure, already available in the literature, but apparently not previously noticed.

MD simulations confirm the structural observations and clearly show that the main polar interactions of T_3 and T_4 in the second site involve Q342 and R375 residues. These features make the second binding site similar to LBP of TRs, especially the TRβ, in which the ligand also interacts with an arginine and a glutamine. However, there are some striking differences between the sites. The second binding site is less hydrophobic and more solvent is exposed in both TRα structures than in the first binding site. Another difference between the 2 sites is the presence of negatively charged residues D328, D336, E339, and E343 (D382, E390, E393, and D397 in TRβ1) near to the amino group of T_3 and T_4, where the interaction can be intermediated by water molecules. The LBP does not show any negatively charged residue in its cavity but shows positively charged residues (R228, R262, and R266 in TRα; R282, R316 and R320, in TRβ1).

It is also important to remark that the ligand is in a different conformation in the second binding site. Previous NMR studies of thyroid hormones in aqueous solutions show that there are 2 major conformations of T_3 and T_4 in water: cisoid and transoid (59, 60). When bound to TRs, T_3 and T_4 assume only one conformation, depending on the binding site: transoid in the LBP and cisoid in the new second binding site. The conversion between the 2 conformations in water occurs in the microsecond time scale (59) and may influence the association mechanisms and kinetics of the ligands in the different binding sites. Finally, our results also highlight the increased mobility of ligands at the second binding site in relation to T_3 in the LBP. The greater mobility of ligands bound to proteins can be an important factor to determine the affinity and/or selectivity for specific binding sites, as demonstrated by the entropic gain of Triac ligand in TRβ1 LBP (8).

These differences in the ligands' conformation, mobility, hydration, and interactions with the LBD can be used for the rational design of drugs that are selective for different TR binding sites. However, prior to this, a better understanding of the affinity and biological function of the natural ligands on the second binding site is necessary. The present study is a first step toward this goal.

MD simulation estimates of thyroid hormones affinities for the second site suggest T_4 as a strong candidate for the natural high-affinity ligand of the second biding site under physiologic conditions. The range of serum and intracellular concentrations of the thyroid hormones (69, 70) also strengthens this hypothesis. However, T_3 should not be discarded as a second-site binder for several reasons: the intracellular concentration of T_3 is usually greater than its plasma concentration (69, 70); the heterogeneity of T_3 concentration in cellular compartments (71), particularly cell nucleus; and the small amount of TR molecules (2,000–10 000) in the cell nucleus (72), which can facilitate the saturation of the LBD binding sites, even at low concentrations of T_3.

Our SCA results and mutant transactivation assays support the existence of a functional network of residues involving the second binding site identified in our crystal structure and other important regions of the LBDs. However, these results do not rule out possible effects caused by these mutations directly in the LBP or their effect in coregulator recruitment and dimerization, or even partial structure destabilization. Indeed, previous studies indicate that mutations relatively distant from the canonical binding site can affect ligand interactions with LBP (73). TRβ mutations in the correspondent residues R429 and Q396 (R375 and Q342 in TRα) caused weak and stronger decreases in nuclear receptor corepressor binding, respectively. In fact, these residues were characterized as "Site 3" for corepressor binding (74). Furthermore, H10 and H11 participate in the formation of TR-TR homodimerization (75) and TR-retinoid X receptor heterodimerization surfaces (76, 77). Thus, a second molecule bound in this region could influence dimer formation.

The double conformation of R228 observed in the crystal structures and MD simulations suggest that ligands in the second binding site can influence ligand-protein interactions in the LBP. It is well established that R228 of TRα (R282 in TRβ1) is very important for ligand affinity and selectivity (77). Furthermore, this residue is involved in the dissociation path III, which, according to

MD simulations, is likely the main ligand exit route from TR LBD (20, 21). Thus, this double conformation may reduce the ligand affinity to and/or facilitate its dissociation from the LBP. In fact, it has been shown that certain ligands, such as GC-24 and T_4, can accelerate the dissociation of T_3 from the LBP. These results were explained by the hypothesis of these ligands anchoring to some different region of LBD, facilitating the dissociation of T_3 from the LBP (14). One possibility is that this different region is the second binding site that we report here.

Another curious fact is that the second binding site is located exactly in the same region where the F domain may dock. F domain is an extension to the C terminus of H12 present in some of the NRs, with an unknown functional role. There is no F domain in human TRs. However, it has been recently found that a TRα isoform from zebrafish does have an F domain (78). Although the structure is unknown, functional assays reveal that the presence of the F domain represses transcriptional activity and reduces the ability to recruit certain coactivators (78). Supplemental Figure 3 shows the LBD structures of the androgen and thyroid receptors aligned, highlighting the F domain of AR and T_3 in the second binding site of TR. The similarity between the positions where the F domain is docked and the second binding site is remarkable. This coincident position suggests a common function for this region: to modulate transcriptional repression.

Thus, it is possible to speculate that the TR's activation may be suppressed by high concentration of the thyroid hormones in the nucleus cell. The excess of hormones leads their association to the second binding site. This could induce ligand dissociation from the LBP (responsible for agonist conformation of H12), thereby reducing gene transcription. Experimental evidence of these ideas was sought after by our group, but technical difficulties prevented us from obtaining reliable results. If this hypothesis proves correct, binding to the second site could be a mechanism to prevent superactivation of TRs, depending on the concentration of ligands.

In summary, the results presented here show a new binding site of the natural thyroid hormones in the TR's LBD. They also indicate that this second binding site may modulate changes in activity and interaction with ligands in the LBP. Nevertheless, binding of a molecule to a second binding site could be useful as a new target for TR drug design and could selectively modulate NR functions.

Acknowledgments

We thank Lucas Bleicher and Larissa C. Textor for helping us with SCA experiments.

Address all correspondence and requests for reprints to: Igor Polikarpov, Universidade de São Paulo, Dept Física e Informática, Instituto de Física, Av. Trabalhador Sãocarlense, 400, São Carlos, SP, Brazil, 13560–970. E-mail: ipolikarpov@ifsc.usp.br.

This work was supported by Fundação de Amparo de Pesquisa do Estado de São Paulo (FAPESP) and Conselho Nacional de Desenvolvimento Científico e Tecnológico (CNPq). M.S.S. was supported through the CEPID Grant 2013/08293–7 from FAPESP. A.C.M.F. was supported by Grant 2010/17048–8 from FAPESP.

Disclosure Summary: The authors have nothing to disclose.

References

1. **Yen P.** Physiological and molecular basis of thyroid hormone action. *Physiol Rev*. 2001;81:1097–10142.
2. **Ribeiro RC, Kushner PJ, Baxter JD.** The nuclear hormone receptor gene superfamily. *Annu Rev Med*. 1995;46:443–453.
3. **Lazar MA, Chin WW.** Nuclear thyroid hormone receptors. *J Clin Invest*. 1990;86:1777–1782.
4. **Wagner R, Huber B, Shiau A, et al.** Hormone selectivity in thyroid hormone receptors. *Mol Endocrinol*. 2001;15:398–410.
5. **Sandler B, Webb P, Apriletti J, et al.** Thyroxine-thyroid hormone receptor interactions. *J Biol Chem*. 2004;279:55801–55808.
6. **Blange I, Drvota V, Yen PM, Sylven C.** Species differences in cardiac thyroid hormone receptor isoforms protein abundance. *Biol Pharm Bull*. 1997;20:1123–1126.
7. **Schwartz HL, Strait KA, Ling NC, Oppenheimer JH.** Quantitation of rat tissue thyroid hormone binding receptor isoforms by immunoprecipitation of nuclear triiodothyronine binding capacity. *J Biol Chem*. 1992;267:11794–11799.
8. **Martínez L, Nascimento AS, Nunes FM, et al.** Gaining ligand selectivity in thyroid hormone receptors via entropy. *Proc Natl Acad Sci USA*. 2009;106:20717–20722.
9. **Bleicher L, Aparicio R, Nunes F, et al.** Structural basis of GC-1 selectivity for thyroid hormone receptor isoforms. *BMC Struct Biol*. 2008;8:8.
10. **Gauthier K, Chassande O, Plateroti M, et al.** Different functions for the thyroid hormone receptors TRα and TRβ in the control of thyroid hormone production and post-natal development. *EMBO J*. 1999;18:623–631.
11. **Johansson C, Vennström B, Thorén P.** Evidence that decreased heart rate in thyroid hormone receptor-α1-deficient mice is an intrinsic defect. *Am J Physiol*. 1998;275:R640–R646.
12. **Weatherman RV, Fletterick RJ, Scanlan TS.** Nuclear-receptor ligands and ligand-binding domains. *Annu Rev Biochem*. 1999;68:559–5581.
13. **Webb P, Nguyen NH, Chiellini G, et al.** Design of thyroid hormone receptor antagonists from first principles. *J Steroid Biochem Mol Biol*. 2002;83:59–73.
14. **Cunha Lima ST, Nguyen NH, Togashi M, et al.** Differential effects of TR ligands on hormone dissociation rates: Evidence for multiple ligand entry/exit pathways. *J Steroid Biochem Mol Biol*. 2009;117:125–131.
15. **Perakyla M.** Ligand unbinding pathways from the vitamin D receptor studied by molecular dynamics simulations. *Eur Biophys J*. 2009;38:185–198.
16. **Sonoda MT, Martínez L, Webb P, Skaf MS, Polikarpov I.** Ligand dissociation from estrogen receptor is mediated by receptor dimerization: Evidence from molecular dynamics simulations. *Mol Endocrinol*. 2008;22:1565–1578.
17. **Martínez L, Polikarpov I, Skaf MS.** Only subtle protein conformational adaptations are required for ligand binding to thyroid hormone receptors: Simulations using a novel multipoint steered mo-

lecular dynamics approach. *J Phys Chem B*. 2008;112:10741–10751.
18. **Genest D, Garnier N, Arrault A, Marot C, Morin-Allory L, Genest M.** Ligand-escape pathways from the ligand-binding domain of PPARγ receptor as probed by molecular dynamics simulations. *Eur Biophys J*. 2008;37:369–379.
19. **Carlsson P, Burendahl S, Nilsson L.** Unbinding of retinoic acid from the retinoic acid receptor by random expulsion molecular dynamics. *Biophys J*. 2006;91:3151–3161.
20. **Martínez L, Webb P, Polikarpov I, Skaf MS.** Molecular dynamics simulations of ligand dissociation from thyroid hormone receptors: evidence of the likeliest escape pathway and its implications for the design of novel ligands. *J Med Chem*. 2006;49:23–26.
21. **Martínez L, Sonoda MT, Webb P, Baxter JD, Skaf MS, Polikarpov I.** Molecular dynamics simulations reveal multiple pathways of ligand dissociation from thyroid hormone receptors. *Biophys J*. 2005;89:2011–2023.
22. **Moras D, Gronemeyer H.** The nuclear receptor ligand-binding domain: structure and function. *Curr Opin Cell Biol*. 1998;10:384–391.
23. **Glass CK, Rosenfeld MG.** The coregulator exchange in transcriptional functions of nuclear receptors. *Genes Dev*. 2000;14:121–141.
24. **Nichols M, Rientjes JM, Stewart AF.** Different positioning of the ligand-binding domain helix 12 and the F domain of the estrogen receptor accounts for functional differences between agonists and antagonists. *EMBO J*. 1998;17:765–773.
25. **Brzozowski AM, Pike AC, Dauter Z, et al.** Molecular basis of agonism and antagonism in the oestrogen receptor. *Nature*. 1997;389:753–758.
26. **Figueira AC, Saidemberg DM, Souza PC, et al.** Analysis of agonist and antagonist effects on thyroid hormone receptor conformation by hydrogen/deuterium exchange. *Mol Endocrinol*. 2011;25:15–31.
27. **Wang Y, Chirgadze NY, Briggs SL, Khan S, Jensen EV, Burris TP.** A second binding site for hydroxytamoxifen within the coactivator-binding groove of estrogen receptor beta. *Proc Natl Acad Sci U S A*. 2006;103:9908–9911.
28. **Hedden A, Müller V, Jensen E.** A new interpretation of antiestrogen action. *Ann NY Acad Sci*. 1995;761:109–120.
29. **Jensen EV, Khan SA.** A two-site model for antiestrogen action. *Mech Ageing Dev*. 2004;125:679–682.
30. **Estébanez-Perpiñá E, Arnold LA, Nguyen P, et al.** A surface on the androgen receptor that allosterically regulates coactivator binding. *Proc Natl Acad Sci USA*. 2007;104:16074–16079.
31. **Lack NA, Axerio-Cilies P, Tavassoli P, et al.** Targeting the binding function 3 (BF3) site of the human androgen receptor through virtual screening. *J Med Chem*. 2011;54:8563–8573.
32. **Munuganti RS, Leblanc E, Axerio-Cilies P, et al.** Targeting the binding function 3 (BF3) site of the androgen receptor through virtual screening. 2. Development of 2-((2-phenoxyethyl) thio)-1H-benzimidazole derivatives. *J Med Chem*. 2013;56:1136–1148.
33. **Mizwicki MT, Keidel D, Bula CM, et al.** Identification of an alternative ligand-binding pocket in the nuclear vitamin D receptor and its functional importance in 1alpha,25(OH)2-vitamin D3 signaling. *Proc Natl Acad Sci U S A*. 2004;101:12876–12881.
34. **Bernardes A, Souza PC, Muniz JR, et al.** Molecular mechanism of peroxisome proliferator-activated receptor α activation by WY14643: a new mode of ligand recognition and receptor stabilization. *J Mol Biol*. 2013;425:2878–2893.
35. **Puhl AC, Bernardes A, Silveira RL, et al.** Mode of peroxisome proliferator-activated receptor γ activation by luteolin. *Mol Pharmacol*. 2012;81:788–799.
36. **Liberato MV, Nascimento AS, Ayers SD, et al.** Medium chain fatty acids are selective peroxisome proliferator activated receptor (PPAR) activators and Pan-PPAR partial agonists. *Plos One*. 2012;7:e36297.
37. **Itoh T, Fairall L, Amin K, et al.** Structural basis for the activation of PPAR by oxidized fatty acids. *Nat Struct Mol Biol*. 2008;15:924–931.
38. **Ambrosio AL, Dias SM, Polikarpov I, Zurier RB, Burstein SH, Garratt RC.** Ajulemic acid, a synthetic nonpsychoactive cannabinoid acid, bound to the ligand binding domain of the human peroxisome proliferator-activated receptor γ. *J Biol Chem*. 2007;282:18625–18633.
39. **Estébanez-Perpiñá E, Arnold LA, Jouravel N, et al.** Structural insight into the mode of action of a direct inhibitor of coregulator binding to the thyroid hormone receptor. *Mol Endocrinol*. 2007;21:2919–2928.
40. **Hwang JY, Arnold LA, Zhu F, et al.** Improvement of pharmacological properties of irreversible thyroid receptor coactivator binding inhibitors. *J Med Chem*. 2009;52:3892–3901.
41. **Hwang JY, Attia RR., Carrillo AK, Connelly MC, Guy RK.** Synthesis and evaluation of methylsulfonylnitrobenzamides (MSNBAs) as inhibitors of the thyroid hormone receptor-coactivator interaction. *Bioorg Med Chem Lett*. 2013;23:1891–1895.
42. **Nunes FM, Aparício R, Santos MA, et al.** Crystallization and preliminary X-ray diffraction studies of isoform α1 of the human thyroid hormone receptor ligand-binding domain. *Acta Crystallogr D Biol Crystallogr*. 2004;60:1867–1870.
43. **Otwinowski Z, Minor W.** Processing of x-ray diffraction data collected in oscillation mode. *Methods Enzymol*. 1997;276:307–326.
44. **Navaza J.** Implementation of molecular replacement in AMoRe. *Acta Crystallogr D Biol Crystallogr*. 2001;57:1367–1372.
45. **Adams PD, Afonine PV, Bunkóczi G, et al.** PHENIX: a comprehensive Python-based system for macromolecular structure solution. *Acta Crystallogr D*. 2010;66:213–221.
46. **Murshudov G, Vagin A, Dodson E.** Refinement of macromolecular structures by the maximum-likelihood method. *Acta Crystallogr D Biol. Crystallogr*. 1997;53:240–255.
47. **Emsley P, Cowtan K.** Coot: model-building tools for molecular graphics. *Acta Crystallogr D Biol Crystallogr*. 2004;60:2126–2132.
48. **Waterhouse AM, Procter JB, Martin DM, Clamp M, Barton GJ.** Jalview Version 2—a multiple sequence alignment editor and analysis workbench. *Bioinformatics*. 2009;25:1189–1191.
49. **Lockless SW, Ranganathan R.** Evolutionarily conserved pathways of energetic connectivity in protein families. *Science*. 1999;286:295–299.
50. **Süel GM, Lockless SW, Wall MA, Ranganathan R.** Evolutionarily conserved networks of residues mediate allosteric communication in proteins. *Nature Struct Biol*. 2003;10:59–69.
51. **Feng W, Ribeiro RC, Wagner RL, et al.** Hormone-dependent coactivator binding to a hydrophobic cleft on nuclear receptors. *Science*. 1998;280:1747–1749.
52. **Martínez L, Andrade R, Birgin EG, Martínez JM.** PACKMOL: A package for building initial configurations for molecular dynamics simulations. *J Comput Chem*. 2009;30:2157–2164.
53. **Martínez JM, Martínez L.** Packing optimization for automated generation of complex system's initial configurations for molecular dynamics and docking. *J Comput Chem*. 2003;24:819–825.
54. **Verlet L.** Computer experiments on classical fluids. I Thermodinamical properties of Lennard-Jones molecules. *Phys Rev*. 1967;159:98–103.
55. **Darden T, York D, Pedersen L.** Particle Mesh Ewald: an Nlog(N) method for Ewald sums in large systems. *J Chem Phys*. 1993;98:10089–10092.
56. **Phillips JC, Braun R, Wang W, et al.** Scalable molecular dynamics with NAMD. *J Comput Chem*. 2005;26:1781–1802.
57. **MacKerell AD Jr , Bashford D, Bellott M, et al.** All-atom empirical potential for molecular modeling and dynamics studies of proteins. *J Phys Chem B*. 1998;102:3586–3616.
58. **Jorgensen WL, Chandrasekhar J, Madura JD, Impey RW, Klein**

ML. Comparison of simple potential functions for simulating liquid water. *J Chem Phys*. 1983;79:926–935.
59. **Duggan BM, Craik DJ.** Conformational dynamics of thyroid hormones by variable temperature nuclear magnetic resonance: the role of side chain rotations and cisoid/transoid interconversions. *J Med Chem*. 1997;40:2259–2265.
60. **Duggan BM, Craik DJ.** ^{1}H and ^{13}C NMR relaxation studies of molecular dynamics of the thyroid hormones thyroxine, 3,5,3′-triiodothyronine, and 3,5-diiodothyronine. *J Med Chem*. 1996;39:4007–4016.
61. **Hansson AO, Souza PCT, Silveira RL, Martínez L, Skaf MS.** CHARMM force field parameterization of rosiglitazone. *Int J Quantum Chem*. 2011;111:1346–1354.
62. **Prates ET, Souza PCT, Pickholz M, Skaf MS.** CHARMM based parameterization of neutral articaine—a widely used local anesthesic. *Intern J Quantum Chem*. 2011;111:1339–1345.
63. **Hénin J, Fiorin J, Chipot C, Klein ML.** Exploring multidimensional free energy landscapes using time-dependent biases on collective variables. *J Chem Theory Comput*. 2010;6:35–47.
64. **Hénin J, Chipot C.** Overcoming free energy barriers using unconstrained molecular dynamics simulations. *J Chem Phys*. 2004;121:2904–2914.
65. **Chipot C, Hénin J.** Exploring the free-energy landscape of a short peptide using an average force. *J Chem Phys*. 2005;123:244906.
66. **Nascimento AS, Dias SM, Nunes FM, et al.** Structural rearrangements in the thyroid hormone receptor hinge domain and their putative role in the receptor function. *J Mol Biol*. 2006;360:586–598.
67. **Wagner RL, Apriletti JW, McGrath ME, West BL, Baxter JD, Fletterick RJ.** A structural role for hormone in the thyroid hormone receptor. *Nature*. 1995;378:690–697.
68. **Borngraeber S, Budny MJ, Chiellini G, et al.** Ligand selectivity by seeking hydrophobicity in thyroid hormone receptor. *Proc Natl Acad Sci USA*. 2003;100:15358–15363.
69. **Escobar-Morreale HF, Obregón MJ, Escobar del Rey F, Morreale de Escobar G.** Replacement therapy for hypothyroidism with thyroxine alone does not ensure euthyroidism in all tissues, as studied in thyroidectomized rats. *J Clin Invest*. 1995;96:2828–2838.
70. **Trost SU, Swanson E, Gloss B, et al.** The thyroid hormone receptor-β-selective agonist GC-1 differentially affects plasma lipids and cardiac activity. *Endocrinology*. 2000;141:3057–3064.
71. **Oppenheimer JH, Schwartz HL.** Stereospecific transport of triiodothyronine from plasma to cytosol and from cytosol to nucleus in rat liver, kidney, brain, and heart. *J Clin Invest*. 1985;75:147–154.
72. **Shahrara S, Drvota V, Sylvén C.** Organ specific expression of thyroid hormone receptor mRNA and protein in different human tissues. *Biol Pharm Bull*. 1999;22:1027–1033.
73. **Souza PC, Barra GB, Velasco LF, et al.** Helix 12 dynamics and thyroid hormone receptor activity: experimental and molecular dynamics studies of Ile280 mutants. *J Mol Biol*. 2011;412:882–893.
74. **Marimuthu A, Feng W, Tagami T, et al.** TR surfaces and conformations required to bind nuclear receptor corepressor. *Mol Endocrinol*. 2002;16:271–286.
75. **Togashi M, Nguyen P, Fletterick R, Baxter JD, Webb P.** Rearrangements in thyroid hormone receptor charge clusters that stabilize bound 3,5′,5-triiodo-L-thyronine and inhibit homodimer formation. *J Biol Chem*. 2005;280:25665–25673.
76. **Ribeiro RC, Feng W, Wagner RL, et al.** Definition of the surface in the thyroid hormone receptor ligand binding domain for association as homodimers and heterodimers with retinoid X receptor. *J Biol Chem*. 2001;276:14987–14995.
77. **de Araujo AS, Martínez L, de Paula Nicoluci R, Skaf MS, Polikarpov I.** Structural modeling of high-affinity thyroid receptor-ligand complexes. *Eur Biophys J*. 2010;39:1523–1536.
78. **Takayama S, Hostick U, Haendel M, Eisen J, Darimont B.** An F-domain introduced by alternative splicing regulates activity of the zebrafish thyroid hormone receptor α. *Gen Comp Endocrinol*. 2008;155:176–189.